

Non-equilibrium steady states of long-range coupled harmonic chains

Francesco Andreucci,¹ Stefano Lepri,^{2,3} Stefano Ruffo,^{1,2} and Andrea Trombettoni^{4,1,5}

¹*SISSA and INFN, Sezione di Trieste, Via Bonomea 265, I-34136 Trieste, Italy*

²*Consiglio Nazionale delle Ricerche, Istituto dei Sistemi Complessi, Via Madonna del Piano 10 I-50019 Sesto Fiorentino, Italy.*

³*Istituto Nazionale di Fisica Nucleare, Sezione di Firenze, via G. Sansone 1, I-50019 Sesto Fiorentino, Italy*

⁴*Department of Physics, University of Trieste, Strada Costiera 11, I-34151 Trieste, Italy*

⁵*CNR-IOM DEMOCRITOS Simulation Center, Via Bonomea 265, I-34136 Trieste, Italy*

We perform a numerical study of transport properties of a one-dimensional chain with couplings decaying as an inverse power $r^{-(1+\sigma)}$ of the intersite distance r and open boundary conditions, interacting with two heat reservoirs. Despite its simplicity, the model displays highly nontrivial features in the strong long-range regime, $-1 < \sigma < 0$. At weak coupling with the reservoirs, the energy flux departs from the predictions of perturbative theory and displays anomalous superdiffusive scaling of the heat current with the chain size. We trace back this behavior to the transmission spectrum of the chain, which displays a self-similar structure with a characteristic sigma-dependent fractal dimension.

I. INTRODUCTION

The main task of statistical mechanics is to relate the microscopic interactions of a given system to its macroscopic properties. One typical instance is the context of heat transfer. Suppose we apply a temperature gradient ∇T to a system, after a while the system will reach a stationary state characterized by the presence of a heat flux \mathcal{J} . The thermal conductivity κ is defined in terms of these quantities as:

$$\mathcal{J} = -\kappa \nabla T, \quad (1)$$

In the case of diffusive transport, Fourier's law holds and κ does not depend on the size of the system N in the thermodynamic limit. This is typically the case for three-dimensional systems with short-range interactions. We remark, however, that there is currently no generic way, given the microscopic properties of a system, to know whether Fourier's law holds or not.

A case in which Fourier's law is systematically violated is the case of harmonic interactions. For instance, for the harmonic crystal each phonon propagates freely and the transport is ballistic. This was showed for the first time for a chain with nearest-neighbors interactions in the seminal paper by Rieder, Lebowitz and Lieb [1]. They found that the thermal conductivity κ diverges as $\kappa \propto N$, N being the number of particles in the chain. Moreover, the bulk temperature profile is flat, while Fourier's law would lead to a linear one. The non-equilibrium properties of quantum harmonic lattices have also been considered in the last decades [2–6].

Generally speaking, in harmonic lattices transport features are dictated by the spectral properties of both the thermal reservoirs and the system itself. For instance in the case of disordered lattices displaying Anderson localization, the conductivity (or energy flux) depends on the localization lengths, but also on the boundary conditions [7], the spectral density of the baths at low frequencies [8] as well as on the distribution and correlations of the

random disorder [9, 10]. For more general, non homogeneous harmonic networks, the spectral properties can be accounted by random matrix theory and can describe also current fluctuations [11]. This is even more striking for active (non-equilibrium) baths that can lead to non-trivial transport regimes even for the ordered harmonic chain [12].

It became progressively become clear that in one (and two) dimensions there are violations of Fourier's law also for nonlinear systems [13–17], such as the Fermi-Pasta-Ulam-Tsingou (FPUT) chain. In one dimension, these violations manifest themselves as a power-law divergence of the thermal conductivity κ with the system's size $\kappa \propto N^\alpha$. Transport in these cases is called anomalous. It is now clear that superdiffusive transport is a generic feature of non-linear one-(and two)-dimensional non-integrable systems conserving momentum, energy and stretch. There are both numerical and analytical evidences that the exponent α can be used to identify different universality classes [16]. For weakly non-integrable models the scenario may be more involved since quasi-particles may have very large mean-free paths [18, 19].

A further element of interest is represented by the presence of forces that are not strictly local. Indeed, much less is known about systems with long-range interactions, that is, systems in which the interparticle interaction scales with the particle distance r as $V(r) \propto r^{-d-\sigma}$. Several physical systems are characterized by long-range interaction, both classical (gravity, pure plasmas, 2d hydrodynamics) and quantum (dipolar systems and trapped atoms). As a concrete experimental instance we mention trapped ion chains, where ions are confined in periodic arrays and interact with external reservoirs [20, 21]. On a macroscale, effective long-range forces arise for tailored macroscopic systems like chain of coupled magnets [22] and the effects of fluctuations and nonlinearity may be relevant.

Long-range systems received considerable attention in the last years, for reviews see for example [23] and [24]

for classical and quantum systems respectively. For what we are going to be concerned with in this paper, we remind that, at equilibrium, the universality class of a one-dimensional long-range system depends on the value of σ . Indeed, for $-1 < \sigma < 0$, the critical exponents are the mean field ones, that is the ones that we obtain by putting $\sigma = -1$. Then, there exists a non universal value σ^* such that for $\sigma > \sigma^*$ we recover the critical exponents of the short-range case $\sigma = \infty$. Typically $\sigma^* > 0$. Furthermore, excitations in long-range systems can propagate at diverging velocity [25, 26] and therefore we can expect some form of superdiffusive transport. There are already several, mainly numerical, studies of heat transport in long-range interacting systems that confirm these expectations. On the classical side, the heat transport was analyzed for the long-range XY model [27, 28] and in the FPUT chain in [28–32] and the lattice φ^4 theory [33]. In all cases Fourier's law is violated in different ways according to the value of σ . Scaling analysis of equilibrium correlations also suggests that hydrodynamics is non-standard [30, 33]. Thus, one may interpret transport as a fractional diffusion process with energy carriers performing Lévy flights, with jump statistics controlled by the exponent σ .

A classical harmonic long-range model with a stochastic dynamics was studied analytically in [34, 35] and the heat flux and temperature profile for a mean-field chain were computed in [36, 37]. The same system was studied in the quantum regime in [37] and a hydrodynamic approach to study transport in quantum magnets was proposed in [38]. We refer again to [24] for more references on the study of dynamics and transport in quantum long-range systems. However, in the literature there is not yet a detailed study of the plain harmonic chain with power-law interaction, and this contribution aims at filling this gap. We will show that the results are far from trivial in the strong long-range case and deserve careful analysis.

More precisely, in this paper we study numerically heat transport in a quadratic chain with a power-law interaction by coupling the first and last site of the system to two heat baths at different temperature. We focus on computing the heat flux in the stationary state with different approaches. In section II we introduce the model and the main methods that we will use to compute the heat flux. In section III–V we report an analysis based on the spectral properties of the nonequilibrium Green's function and the transmission spectra and we discuss them. Finally, we draw our conclusions in section VI.

II. MODEL AND METHODS

A. The long-range coupled harmonic chain

We consider a one-dimensional chain of particles with a power-law interaction:

$$H = \frac{1}{2} \sum_i p_i^2 + \frac{1}{2} \sum_{ij} x_i \Phi_{ij} x_j, \quad (2)$$

where the interaction matrix Φ is given by:

$$\Phi_{ij} = \left(2\delta_{ij} - \frac{1}{N_\sigma} \frac{1}{|i-j|^{1+\sigma}} \right), \quad N_\sigma = \sum_{l=1}^N l^{-\sigma}, \quad (3)$$

where N_σ is the usual Kac factor introduced to guarantee extensivity of the energy, chosen as site-independent. The matrix correctly reduces to the discrete Laplacian for large σ . Note that definition (3) corresponds to open boundary conditions, which are the ones appropriate for our problem due to the presence of the baths. For long-ranged systems we expect that the role of boundary conditions can have very important consequences, even more than for short-ranged systems, and we focus on this natural choice for simplicity.

In the case of open boundary conditions the spectrum of matrix Φ is, to the best of our knowledge, not known analytically. The usual standing waves are not eigenvectors and the matrix cannot be diagonalized exactly. Even in the continuum limit, this would correspond to solving the spectral problem for the fractional Laplacian in a finite domain, which is notoriously not straightforward [39].

For comparison, it is useful to recall the solvable case for periodic boundary condition where the proper definition of Φ is:

$$\Phi_{ij} = \left(2\delta_{ij} - \frac{1}{N_\sigma \min(N - |i-j|^{1+\sigma}, |i-j|^{1+\sigma})} \right). \quad (4)$$

Here the spectrum is known, see for example [40]. Due to translational invariance, the eigenvectors are plane waves of wavenumber k . The nature of the eigenfrequency spectra strongly depends on whether σ is positive or negative. In the first case, the system has a proper continuum limit and for low momenta k the squared frequencies ω^2 of the plane waves behave as:

$$\omega_k^2 \approx \begin{cases} |k|^\sigma, & 0 < \sigma < 2, \\ k^2, & \sigma > 2. \end{cases} \quad (5)$$

Thus, for $\sigma > 0$ one has the standard acoustic dispersion and a finite group velocities while the group velocity diverges as $|k|^{\frac{\sigma-2}{2}}$ in the first case. This result can also be derived from the continuum limit, corresponding to a fractional wave equation in the infinite domain [41]. On the other hand, if $\sigma < 0$ the spectrum remains discrete

even in the thermodynamic limit and contains a countable infinite number of frequencies that accumulate at the band edge [40].

To simulate the non-equilibrium steady state, we follow the usual procedure and connect the first and last sites of the system to two Langevin heat baths at temperatures T_L and T_R , respectively. The coupling with the baths introduces both noise and dissipation in the dynamics of the system. The resulting equations of motion are:

$$\ddot{x}_i = - \sum_j \Phi_{ij} x_j + \delta_{i1} (\xi_L - \lambda \dot{x}_i) + \delta_{iN} (\xi_R - \lambda \dot{x}_i), \quad (6)$$

where the ξ 's are Gaussian noises that satisfy the fluctuation-dissipation relation:

$$\langle \xi_a(t) \xi_a(t') \rangle = 2T_a \lambda \delta(t - t'), \quad a = L, R. \quad (7)$$

After a transient, the system reaches a stationary state: we are interested in the heat flux and the temperature profile of the chain in this state. To compute these quantities, we will employ three different methods.

B. RLL approach

The first method was introduced long time ago in this context in [1]. It consists in solving the many-body Fokker-Planck equation related to (6) (in the following we will refer to this method as the RLL method). In particular, defining the vector $y = (x_1, \dots, x_N, p_1, \dots, p_N)$, and denoting by $P(y, t)$ its probability at time t , the aforementioned equation reads as:

$$\frac{\partial P(y, t)}{\partial t} = A_{ij} \frac{\partial}{\partial y_i} (y_j P) + \frac{1}{2} D_{ij} \frac{\partial^2 P}{\partial y_i \partial y_j}, \quad (8)$$

where the drift and diffusion matrices are

$$A = \begin{pmatrix} \mathbb{O} & -\mathbb{I} \\ -\Phi & \lambda \mathcal{R} \end{pmatrix}, \quad D = \begin{pmatrix} \mathbb{O} & \mathbb{O} \\ \mathbb{O} & 2k_B \lambda T (\mathcal{R} + \eta \mathcal{S}) \end{pmatrix}, \quad (9)$$

where

$$\begin{cases} T = \frac{T_L + T_R}{2}, \\ \eta = \frac{T_L - T_R}{T} \end{cases}, \quad \mathcal{R}_{ij} = \delta_{ij} (\delta_{i1} + \delta_{iN}), \quad (10)$$

$$\mathcal{S}_{ij} = \delta_{ij} (\delta_{i1} - \delta_{iN}). \quad (11)$$

The solution of equation (8) is a multi-variate Gaussian whose covariance matrix is given by the matrix of correlations among the canonical coordinates:

$$P(y, t) \propto \exp \left\{ -\frac{1}{2} C_{ij}^{-1} y_i y_j \right\}, \quad C = \begin{pmatrix} \langle x_i x_j \rangle & \langle x_i p_j \rangle \\ \langle p_i x_j \rangle & \langle p_i p_j \rangle \end{pmatrix}. \quad (12)$$

By plugging (12) in the Fokker-Planck equation (8) we get:

$$\partial_t C = D - AC - CA^T. \quad (13)$$

Furthermore, in the stationary state $\partial_t C = 0$, so we get the so-called (continuous) Lyapunov equation:

$$AC + CA^T = D, \quad (14)$$

which has to be solved numerically. Knowing the various correlators, we can then express the heat flux in the stationary state as the difference between the temperature of the left bath and the temperature of the first site:

$$\mathcal{J} = \lambda (T_L - T_1), \quad T_i = \frac{1}{2} \langle p_i^2 \rangle. \quad (15)$$

C. Nonequilibrium Green's function

The second method consists in writing the exact solution to (6) in terms of the Green's function $G(\omega)$, which is possible due to the linearity of the equations. The details of this method are explained in refs. [3, 14, 42]. Since we are interested in the stationary state, we work directly in frequency space:

$$\tilde{x}_l(\omega) = \sum_{ln} G_{ln}(\omega) (\tilde{\xi}_{L,n}(\omega) + \tilde{\xi}_{R,n}(\omega)), \quad (16)$$

$$G(\omega) = (-\omega^2 \mathbb{I} + \Phi + i\lambda\omega \mathcal{R})^{-1}, \quad (17)$$

where the tilde indicates the Fourier transform and \mathcal{R} is the matrix defined in Eqs.(9, 11). As explained in [14], we can express the heat flux in the stationary state as:

$$\mathcal{J} = \frac{2\Delta T \lambda^2}{\pi} \int_0^\infty d\omega \omega^2 |G_{1N}(\omega)|^2. \quad (18)$$

D. Generalized eigenvalue method

There is in the literature another approach to the Green's function method, called *generalized eigenvalues method*, which we briefly outline below (for a more detailed explanation see [43–45]). Let $G^L(s)$ be the Green's function defined in Laplace's space:

$$G^L(s) = (-s^2 \mathbb{I} + \Phi + \lambda s \mathcal{R})^{-1}, \quad (19)$$

and introduce the $2N$ complex numbers $\{s_a\}_{a=1}^{2N}$ and the $2N$ vectors $\{\mathbf{r}_a\}_{a=1}^{2N}$ as defined by the following linear problem:

$$G^L(s_a) \mathbf{r}_a = 0. \quad (20)$$

Then, the Green's function (19) can be written as [45]:

$$G^L(s) = \sum_{a=1}^{2N} \frac{s_a}{s - s_a} \mathbf{r}_a \mathbf{r}_a^\dagger. \quad (21)$$

Note that the s_a come in complex conjugate pairs. We now recall that we can obtain the Green's function in frequency space $G(\omega)$ via a Wick rotation $G(\omega) = G^L(-is)$.

Then we can compute the integral in (18) with a contour integration one finding [43]:

$$\mathcal{J} = 2\Delta T \lambda^2 \sum_{a,b=1}^{2N} \frac{s_a^3 s_b}{s_a + s_b} r_{a,1} r_{a,N} r_{b,N} r_{b,1}. \quad (22)$$

Formula (22) gives yet another way of computing the heat flux and extract the scaling exponents.

E. Comments

Before proceeding, let us comment on the numerical issues connected with the above approaches. The numerical implementation of the RLL method is rather straightforward resorting to the numerical routines available to solve the Lyapunov equation based on the Bartels-Stewart algorithm, as implemented for instance in the SciPy library [46]. Indeed, one can easily reach sizes of $N \sim 10^3$. Some convergence issues may arise in the case of strong degeneracies [37]. The numerical implementation of the Green's function method can be more involved than the one of the RLL method. Indeed, we need to numerically invert the matrix in the definition of the Green's function (17) in the range of ω where the transmission is non-vanishing in order to be able to compute the integral in (18). Furthermore, the sampling over ω has to be fine enough to ensure accuracy, especially if the transmission coefficient oscillates rapidly. This difficulty does occur in our model, as it will be clear in what follows. In practice, it is difficult to study lattices larger than $N \sim 10^2$ using this method. The generalized eigenvalues method has the advantage of reducing the problem to the calculation of the eigenvalues and eigenvectors of a $2N \times 2N$ matrix [44], which can be done by standard linear algebra routines, the main limitation being memory storage and accuracy of very small eigenvalues and avoiding the sampling problem.

III. HEAT FLUX

In the short-range case, $\sigma = \infty$, two of the methods outlined above have been used to obtain exact analytical results for the heat flux in the thermodynamic limit [1, 14]. This is possible because the matrix of the interactions Φ reduces to the discrete Laplacian, which is a tridiagonal matrix. In our case the matrix Φ is dense, and we are unable to either solve analytically the Lyapunov equation or to exactly compute the Green function. Nonetheless, it is possible to obtain a certain amount of informations about the heat flux numerically.

A. Small coupling

If the coupling with baths λ is small, a perturbative calculation of the steady-state current is possible in terms

of the eigenvalues and eigenvectors of the isolated harmonic chain. This approach yields the so-called Matsuda-Ishii's formula, whereby $\mathcal{J} \approx \mathcal{J}_{MI}$ to the leading order in the coupling constant [13, 47], with \mathcal{J}_{MI} given by

$$\mathcal{J}_{MI} = \lambda \Delta T \sum_k \frac{\psi_{k,1}^2 \psi_{k,N}^2}{\psi_{k,1}^2 + \psi_{k,N}^2} \quad (23)$$

where $\Delta T = T_L - T_R$ and $\psi_{k,n}$ denotes the n component of the k th eigenvector of the matrix Φ defined in (3). For the model we consider here (which is homogeneous and mirror-symmetric) the above expression simplifies to

$$\mathcal{J}_{MI} = \frac{\lambda \Delta T}{2} \quad (24)$$

which expresses the fact that the chain is a ballistic conductor.

Typically, in the short-range case $\sigma \rightarrow \infty$, this result applies for $\lambda \ll \lambda_0 \approx \mathcal{O}(1)$. In the our long-range case, however, the situation is more complicated. In Fig. 1, we compare formula (24) and the numerical solution of the Lyapunov equation. As we can see, (24) holds for λ smaller than a certain threshold $\lambda_0(\sigma, N)$, that depends both on N and on σ . More specifically, λ_0 decreases with σ and with N . On the other hand, for $\sigma > 0$ the perturbative approximation holds well in the considered range.

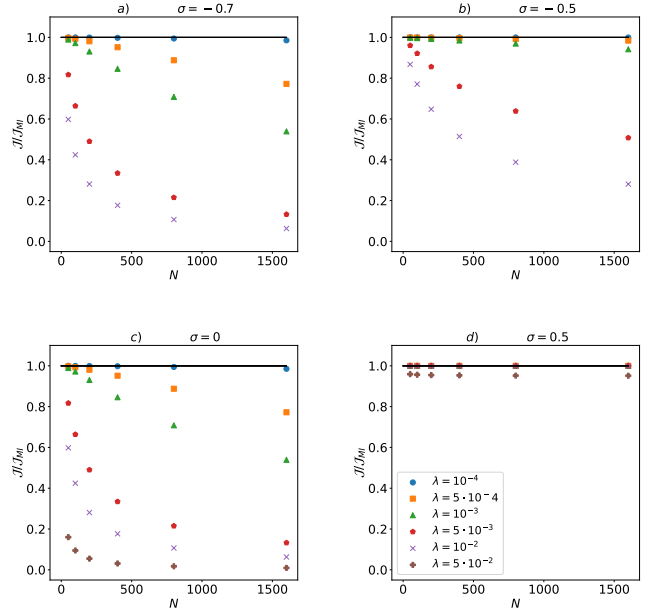


FIG. 1. Plots of the ratio between the heat flux \mathcal{J} , computed numerically with the RLL method, and the Matsuuda-Ishii heat flux (24) versus the system size N for several values of σ and λ in the weak coupling regime.

To have some insight into these deviations we may perform some further checks. Usually the perturbative approach is justified assuming that the separation of the unperturbed normal mode frequencies is smaller than the

typical dissipation caused by the coupling with the baths [43]. This assumption can actually be checked by examining the poles s_a . In particular, we compare the spacings between the imaginary parts of consecutive poles $Im(s_{a+1} - s_a)$ and the real parts $Re(s_a)$. As we can see from Fig. 2, the former is always much larger than the latter, therefore this assumption is justified. This suggests that the observed deviations from the Matsuda-Ishii formula may have a different origin.

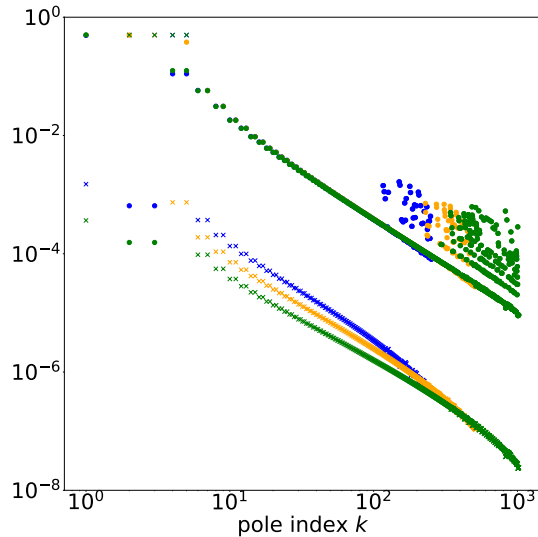


FIG. 2. Plots of the spacing between the imaginary parts of the poles of the Green's function $Im(s_{k+1}) - Im(s_k)$ (circles) and the real parts of the poles $Re(s_k)$ (crosses) for $\sigma = -0.5$. Different colors correspond to different system's size: $N = 256, 512, 1024$ in blue, orange, green, respectively.

B. Strong coupling

We now want to understand how the flux scales with the system size N for not too weak coupling λ . In order to do so, we computed the heat flux using the RLL method for several values of N and σ for $\lambda = 1$ (and we will set $\lambda = 1$ for the rest of the paper). As shown in Fig. 3 the data can be fitted with a power law $\mathcal{J} \propto N^{-\gamma}$.

Although the direct computation of the Green's function is numerically cumbersome, we can easily compute its poles, compute the heat flux according to (22) and fit a power law as we did before. In panel *b*) of Fig. 4 we report both the exponents fitted with the generalized eigenvalues method and with the RLL method. As we can see, they are qualitatively in agreement.

The results of fits using the two methods are reported in Fig. 4. We can identify three regions. The region close to the mean-field case $\sigma = -1$ and the one close to the short-range case $\sigma > 1$, where finite-size effects

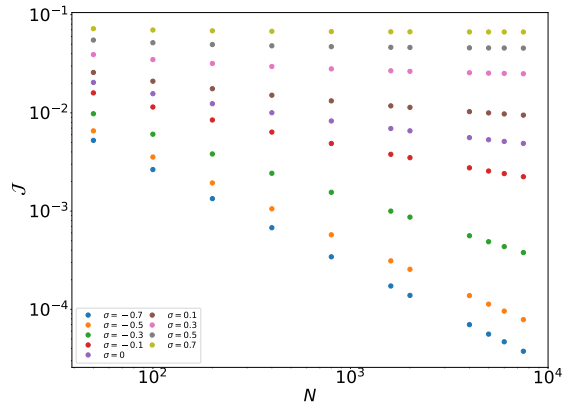


FIG. 3. Log-log plot of the heat flux \mathcal{J} versus the system's size N for $\lambda = 1$ and different values of the long-range exponent σ . The flux is computed using the RLL method as described in the text.

are almost absent, and an intermediate region in which finite-size effects are quite strong. We also note that γ seems to be converging to the short-range value $\gamma = 0$ while σ goes to 1. Summarizing, even if we are not able to extract the exact values of the exponents, it is clear that the flux scales with some nontrivial power of the system's size N .

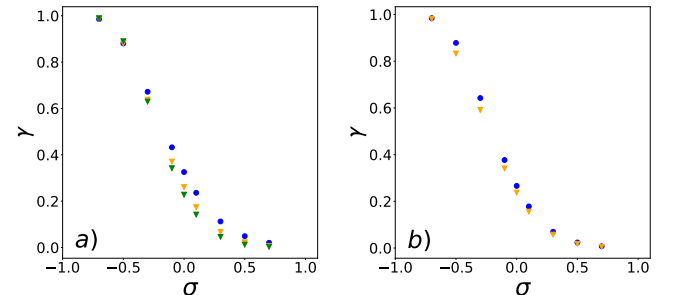


FIG. 4. Plot of the scaling exponent of the flux γ , defined as $\mathcal{J} \propto N^{-\gamma}$, (a), we report the exponents obtained by fitting a power law on the heat flux obtained with the RLL method. To check the finite-size effects, each data set corresponds to a fit over different length ranges, $50 \leq N \leq 1600$ (circles), $500 \leq N \leq 2000$ (squares), $1500 \leq N \leq 7500$ (triangles). Panel (b), comparison between the exponents obtained by the RLL method (circles) and the generalized eigenvalue method (triangles).

IV. TRANSMISSION SPECTRA

To understand the origin of the nontrivial dependence of the flux on the size, let us investigate the transmission spectrum of the chain. We begin by plotting the

transmission coefficient, namely the integrand in (18) as a function of the frequency ω . In Fig. 5 we report its plot for several values of σ . We can see that it is characterized by a rather complicated peak structure which consists of $N - 2$ peaks (as can be checked numerically).

A main point we want to make and explore is that the structure of such resonances determines the scaling of the current. Notice that a change of sign in ω in (17) is equivalent to the complex conjugation of $G(\omega)$. Since the transmission coefficient depends on the square modulus of $G(\omega)$ it is an even function of ω and we can therefore restrict ourselves to study positive frequencies. Let us denote by ω_k , $k = 1, 2, \dots$ the location of the peak frequencies for positive ω . The peaks accumulate at a band-edge frequency $\omega_B < 2$, i.e. $\omega_k \rightarrow \omega_B$ for k large. Furthermore, upon approaching ω_B , the width of the peaks decreases. Notice that this is the reason why it is important to finely sample the Green's function in ω , especially in the proximity of the band edge. Indeed, we used a logarithmic sampling in order to increase the sampling points near ω_B . The integrand is thus a much more complicated function of ω with respect to the mean-field case $\sigma = -1$ [36, 37], where only the first peak is present. It can be checked numerically that the first few peaks are Lorentzian with amplitude $\Delta_k \approx N^{-1}$, exactly like the peak in mean-field case. The subsequent peaks are too narrow to be resolved. For positive values of σ the situation becomes even more complicated, as a curve emerges below the peaks, as we can see in Fig. 5 for $\sigma = 0.5$.

For the reasons outlined above, it seems more convenient to consider the cumulative function $F(\omega)$, that is, the integral (18) performed up to frequency ω . In the rightmost panels of Fig. 5 we report the function $F(\omega)$ for several values of N of order 10^2 and σ , rescaled by N^γ , where γ is the exponent obtained with the RLL method for values of N of order $10^2 : 10^3$. As we can see, the curves nicely collapse for $\sigma = -0.7, -0.5$, but for higher values of σ , such as $\sigma = -0.3$, the collapse is not as good due to the finite-size effects, as expected. Regardless of the lack of further quantitative progress in the computation of the exponents, the qualitative information about the peak structure will be crucial in our understanding of the model, as we will see later.

V. POLES OF THE GREEN'S FUNCTION

In view of the numerical difficulties encountered above and for comparison, we also performed a study of poles of the Green's function. These are computed through the generalized eigenvalue method described above.

The main advantage of the analysis is that we gain a new perspective on the peak structure discussed before. Indeed, the positions ω_k of the peaks in Fig. 5 are given by the absolute value of the imaginary part of s_a , while the absolute value of the imaginary part should be proportional to their widths Δ_k .

In particular, we consider all the peaks as Lorentzian

– for simplicity, but also because all the peaks that we were able to resolve are actually very well approximated by Lorentzian – with width given by $Re(s_a)$. In this approximation, as far as scaling with the size is concerned, the heat flux can be estimated as the sum of the widths of the peaks $\Delta_k(N)$:

$$\mathcal{J}(N) \approx \sum_{k=1}^{N-2} \Delta_k(N). \quad (25)$$

The relevant information should thus be contained in the dependence of the Δ_k on k and N . Physically, this is the effective damping of plane waves due to the coupling with the thermal reservoirs.

The dependence of Δ_k on N is reported in Fig. 6, where we plot (parametrically) the real parts of the poles as a function of the imaginary ones, for negative and positive values of σ , respectively. Since the resonances accumulates at the band-edges, it is convenient to report the frequencies as a function of their relative distance from ω_B . Let us focus on the case of negative σ , to begin with. From the leftmost panels of Fig. 6, it is seen that the poles can be grouped in two sets, each having different dependencies on ω_k and N . Empirically, this is accounted for by the following scaling:

$$\Delta_k(N) \approx \begin{cases} d_k/N, & k < k_o \\ d_k/N^\delta, & k > k_o, \end{cases} \quad (26)$$

where $k_o \ll N$ and d_k do not depend N . We do not have an a-priori theoretical estimate of δ , but we find that there is a good collapse upon choosing $\delta \approx 1 + |\sigma|$. It is interesting to point out that the exponent δ can be interpreted as the fractal dimension of area below the graphs in Fig. 5. Indeed, if we increase the system's size N new peaks emerge with progressively shrinking area and, in a putative $N \rightarrow \infty$ limit we would have an infinite number of peaks with vanishing area.

In addition, there are a few poles whose widths do not follow this scaling and fall consistently well outside the collapsed curve. It actually turns out that there are two degenerate eigenvalues between the s_a s that do not follow the scaling law. However this is inconsequential, as one can check that the contribution of the these eigenvalues to (22) vanishes. Heuristically, this is because, as one can check, the eigenvectors related to these eigenvalues are localized at the endpoints of the chain and therefore do not contribute to transport. This also explains why the peaks in Fig. 5 are $N - 2$ instead of N . We can therefore infer the following scaling law for the heat flux (22):

$$\mathcal{J} \approx \frac{\sum_{k=1}^{k_o} d_k}{N} + \frac{\sum_{k=k_o}^N d_k}{N^\delta} \propto N^{1-\delta}. \quad (27)$$

For positive σ , the scaling of Δ_k is reported in the right-most panels of Fig. 6: as we can see in this case

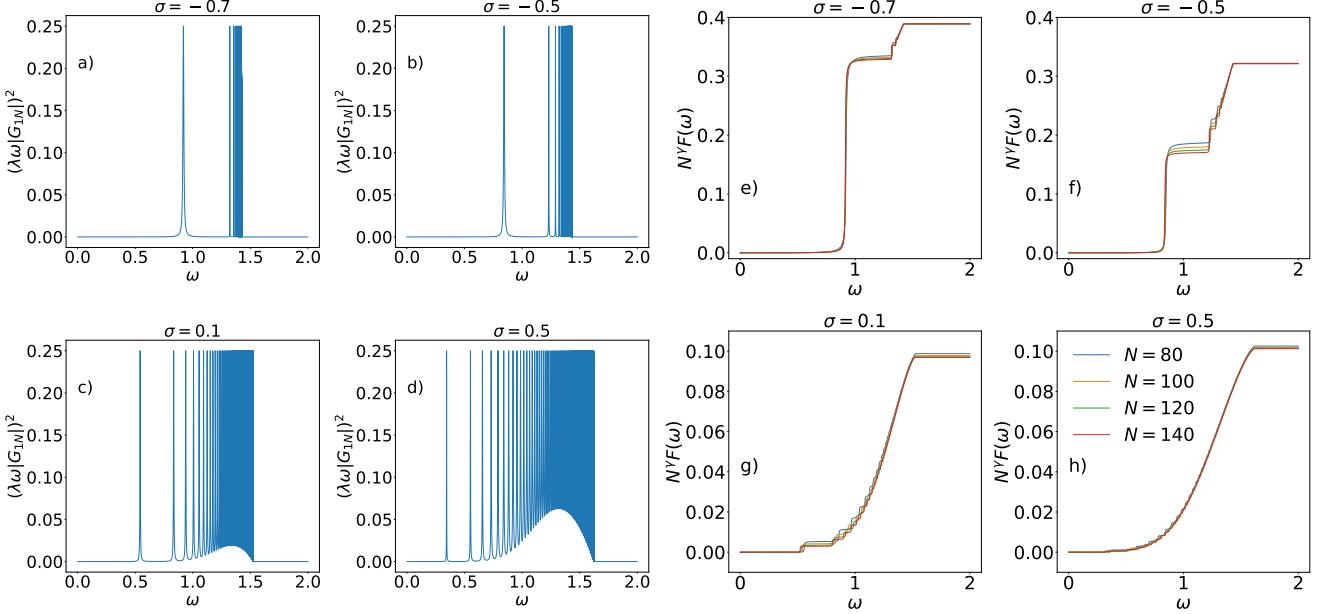


FIG. 5. Panels a), b), c), d) : transmission spectrum (the integrand of the heat flux expression (18)) for different values of the range exponent $\sigma = -0.7, 0.5, 0.1, 0.5$ and for a chain with $N = 100$. Only positive frequencies are reported. Panels e), f), g), h): rescaled cumulative function $N^\gamma F(\omega)$, for $N = 80, 100, 120, 140$ and $\sigma = -0.7, -0.5, -0.1, 0.5$ in panels a), b), c), d) respectively. The values of γ are taken from the blue points in Figure 4.

$\Delta_k \approx N^{-1}$, over the entire spectrum. Therefore, the estimate the heat flux yields

$$\mathcal{J} \approx \frac{\sum_{k=1}^N d_k}{N} \approx \mathcal{O}(1). \quad (28)$$

So the heat flux for positive σ behaves as the heat flux for $\sigma = \infty$ (the nearest-neighbors case), that is, it does not scale with N .

To summarize, according to approximation (25) and the numerical estimate of δ extracted from the data, we find that the heat flux scale as:

$$\mathcal{J} \propto N^{-\tilde{\gamma}}, \quad \tilde{\gamma} \approx \begin{cases} 1 - \delta, & \sigma < 0, \\ 0, & \sigma > 0. \end{cases} \quad (29)$$

As we already mentioned, see Fig. 6, we found a good collapse of the imaginary part of the poles of the Green's functions for $\delta \approx 1 - |\sigma|$. So this yields

$$\tilde{\gamma} \approx -\sigma \quad (30)$$

for negative σ . Admittedly, this estimate accounts only qualitatively for the behavior of the exponents as given in Fig. 4. The deviations are sizeable and, in addition the dependence of γ on σ appears to be non-linear. While this could be due to the aforementioned finite-size effects, the discrepancy is present even for values of σ for which the exponent γ has basically converged (for example $\sigma = -0.7, -0.5$). Another possibility, which seems more likely, is that, while the widths of the peaks of Fig.

5 are indeed related to the real parts of s_a on general grounds, they are not exactly equal. On the other hand, we point out that, since the s_a are related to the widths of the peaks, the transition in the scaling of the Δ_k s at $\sigma = 0$ suggests that the scaling of the heat-flux between the short-range and the long-range behaviour has to occur at $\sigma = 0$.

VI. CONCLUSIONS

Heat transport in short-range linear systems has been widely studied [13]. On the contrary, the behaviour of linear oscillators with long-range power-law couplings is not yet well understood beyond the mean-field (fully-coupled) case [36, 37]. In this paper, we have made a step forward along this direction by applying three different methods [1, 6, 14] that allow to compute numerically both the heat flux and its scaling with the system's size. All the methods give a clear scaling of the current with a power-law in the system's size. This scaling interpolates between the short-range behaviour, where the current is constant in the system's size, and the mean-field behaviour, where the current is inversely proportional to the system's size. However, the fitted scaling exponents show significant finite-size effects for all the three methods. The method of ref. [1] which consists in solving a matricial equation is straightforwardly applicable to the long-range case. The Green's function approach allows to express the current as an integral

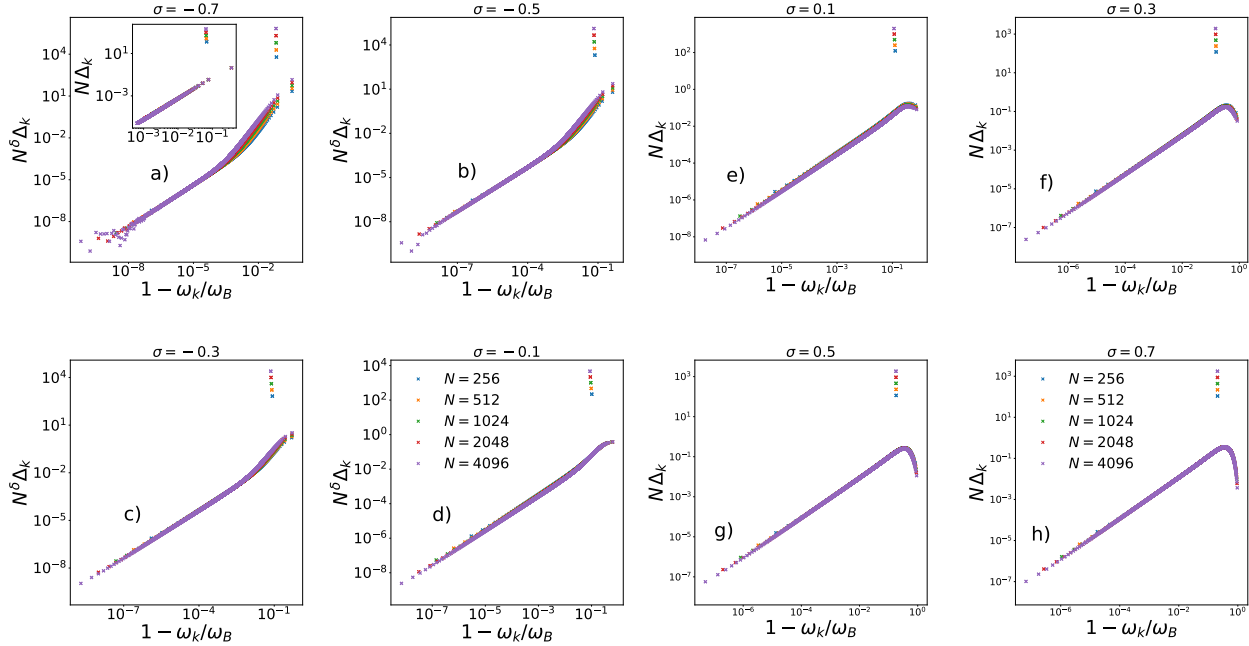


FIG. 6. Real parts of the poles of the Green's functions s_a versus the distance of their imaginary parts from the band-edge. Leftmost panel: $\sigma < 0$, vertical axis rescaled by N^δ with $\delta \approx 1 - \sigma$. The inset in panel (a) demonstrates the different scaling the collapse for the widths of the first peaks (the first 80, 160, 320, 640, 1280 for $N = 256, 512, 1024, 2048$, respectively) rescaled by N . For the other values of σ , we get the same scaling for the first peaks. Rightmost panel: same for $\sigma > 0$, with vertical axis rescaled by N . Note that such scaling works for the whole spectrum in this case.

over frequencies, which cannot be solved analytically. However, the integrand has the interesting property of showing a sequence of peaks that accumulate near the band edges of the spectrum. Further properties of these peaks can be inferred using the third method, which allows to compute the poles of the Green's function. Indeed, the real and the imaginary part of these poles are related to the position and the width of the peaks, respectively. We find a sharp transition in the scaling of the real parts of the poles at the value of the long-range coupling exponent $\sigma = 0$ corresponding to the transition between the long-range and the short-range behaviour of the system. The crucial problem is now the dependence on σ of the scaling exponent of the current. Assuming that all of the peaks of the integrand are well-separated Lorentzians and that their widths are exactly given by the real parts of the poles, we might conclude that the heat current scales as $\mathcal{J} \propto N^{-|\sigma|}$ for $-1 < \sigma < 0$. *cin*

agreement with the one derived directly from the fit of the current, which is anyway affected – at least for small values of $|\sigma|$ – by significant finite-size effects. The disagreement between these two scaling exponents remains to be explored, even though our analysis of the scaling of the real part of the poles of the Green's function clearly supports the presence of a transition at $\sigma = 0$ from the long-range to the short-range behaviour.

ACKNOWLEDGMENTS

We gratefully thank Celia Anteneodo and Lucianno Defaveri for useful discussions. SL and SR acknowledge partial support from project MIUR-PRIN2017 *Coarse-grained description for non-equilibrium systems and transport phenomena (CO-NEST)* n. 201798CZL.

-
- [1] Z. Rieder, J. L. Lebowitz, and E. Lieb, *Journal of Mathematical Physics* **8**, 1073 (1967).
- [2] U. Zürcher and P. Talkner, *Physical Review A* **42**, 3278 (1990).
- [3] A. Dhar and D. Roy, *Journal of Statistical Physics* **125**, 801 (2006)).
- [4] K. Saito, S. Takesue, and S. Miyashita, *Physical Review E* **61**, 2397 (2000).
- [5] A. Asadian, D. Manzano, M. Tiersch, and H. Briegel, *Physical Review E* **87**, 012109 (2013).
- [6] N. Freitas and J. P. Paz, *Physical Review E* **90**, 042128 (2014).

- [7] W. M. Visscher, *Progress of Theoretical Physics* **46**, 729 (1971).
- [8] A. Dhar, *Physical review letters* **86**, 5882 (2001).
- [9] I. Herrera-González, F. Izrailev, and L. Tessieri, *Euro-
physics Letters* **110**, 64001 (2015).
- [10] B. Ash, A. Amir, Y. Bar-Sinai, Y. Oreg, and Y. Imry, *Phys. Rev. B* **101**, 121403 (2020).
- [11] M. Schmidt, T. Kottos, and B. Shapiro, *Physical Review E* **88**, 022126 (2013).
- [12] I. Santra and U. Basu, *SciPost Phys.* **13**, 041 (2022).
- [13] S. Lepri, R. Livi, and A. Politi, *Physics Reports* **377**, 1 (2003).
- [14] A. Dhar, *Adv. Phys.* **57**, 457 (2008).
- [15] S. Lepri, R. Livi, and A. Politi, in *Thermal transport in low dimensions: From statistical physics to nanoscale heat transfer* (Springer, 2016) pp. 1–37.
- [16] G. Benenti, S. Lepri, and R. Livi, *Frontiers in Physics* **8**, 292 (2020).
- [17] G. Benenti, D. Donadio, S. Lepri, and R. Livi, *La Rivista del Nuovo Cimento* **46**, 105 (2023).
- [18] P. Di Cintio, S. Iubini, S. Lepri, and R. Livi, *Chaos, Solitons & Fractals* **117**, 249 (2018).
- [19] S. Lepri, R. Livi, and A. Politi, *Phys. Rev. Lett.* **125**, 040604 (2020).
- [20] A. Bermúdez, M. Bruderer, and M. B. Plenio, *Physical review letters* **111**, 040601 (2013).
- [21] M. Ramm, T. Pruttivarasin, and H. Haeffner, *New Journal of Physics* **16**, 063062 (2014).
- [22] M. Molerón, C. Chong, A. J. Martínez, M. A. Porter, P. G. Kevrekidis, and C. Daraio, *New Journal of Physics* **21**, 063032 (2019).
- [23] A. Campa, T. Dauxois, and S. Ruffo, *Phys. Rep.* **480**, 57 (2009).
- [24] N. Defenu, T. Donner, T. Macrì, G. Pagano, S. Ruffo, and A. Trombettoni, (2021), arXiv:2109.01063 [cond-mat.quant-gas].
- [25] A. Torcini and S. Lepri, *Phys. Rev. E* **55**, R3805 (1997).
- [26] D. Métivier, R. Bachelard, and M. Kastner, *Phys. Rev. Lett.* **112**, 210601 (2014).
- [27] C. Olivares and C. Anteneodo, *Phys. Rev. E* **94**, 042117 (2016).
- [28] S. Iubini, P. Di Cintio, S. Lepri, R. Livi, and L. Casetti, *Phys. Rev. E* **97**, 032102 (2018).
- [29] D. Bagchi, *Phys. Rev. E* **95**, 032102 (2017).
- [30] P. Di Cintio, S. Iubini, S. Lepri, and R. Livi, *Journal of Physics A: Mathematical and Theoretical* **52**, 274001 (2019).
- [31] J. Wang, S. V. Dmitriev, and D. Xiong, *Physical Review Research* **2**, 013179 (2020).
- [32] D. Bagchi, *Physical Review E* **104**, 054108 (2021).
- [33] S. Iubini, S. Lepri, and S. Ruffo, *Journal of Statistical Mechanics: Theory and Experiment* **2022**, 033209 (2022).
- [34] S. Tamaki and K. Saito, *Phys. Rev. E* **101**, 042118 (2020).
- [35] H. Suda, *Nonlinearity* **35**, 2288 (2022).
- [36] L. Defaveri, C. Olivares, and C. Anteneodo, *Phys. Rev. E* **105**, 054149 (2022).
- [37] F. Andreucci, S. Lepri, S. Ruffo, and A. Trombettoni, *SciPost Phys. Core* **5**, 036 (2022).
- [38] A. Schuckert, I. Lovas, and M. Knap, *Phys. Rev. B* **101**, 020416 (2020).
- [39] A. Zoia, A. Rosso, and M. Kardar, *Physical Review E* **76**, 021116 (2007).
- [40] N. Defenu, *Proceedings of the National Academy of Sciences* **118**, e2101785118 (2021).
- [41] V. E. Tarasov, *Journal of Physics A: Mathematical and General* **39**, 14895 (2006).
- [42] A. Dhar and K. Saito, in *Thermal Transport in Low Dimensions* (Springer, 2016) pp. 39–105.
- [43] N. Freitas and J. P. Paz, *Phys. Rev. E* **90**, 042128 (2014).
- [44] N. Freitas, E. A. Martinez, and J. P. Paz, *Physica Scripta* **91**, 013007 (2015).
- [45] F. Tisseur and K. Meerbergen, *SIAM Review* **43**, 235 (2001), <https://doi.org/10.1137/S0036144500381988>.
- [46] P. S. Virtanen et al., *Nature Methods* **17**, 261 (2020).
- [47] H. Matsuda and K. Ishii, *Progress of Theoretical Physics Supplement* **45**, 56 (1970).